Caenorhabditis elegans models for striated muscle disorders caused by missense variants of human *LMNA*

Ellen F. Gregory[1], Shilpi Kalra[1], Trisha Brock[2], Gisèle Bonne[3], G.W. Gant Luxton[1], Christopher Hopkins[2], Daniel A. Starr[1*]

[1]Department of Molecular and Cellular Biology, University of California, Davis, CA, USA

[2]InVivo Biosystems, Eugene, OR, USA

[3]Sorbonne Université, Inserm, Institut de Myologie, Centre de Recherche en Myologie, Paris, France

*Corresponding author

E-mail: dastarr@ucdavis.edu (DAS)

Abstract

Striated muscle laminopathies caused by missense mutations in the nuclear lamin gene *LMNA* are characterized by cardiac dysfunction and often skeletal muscle defects. Attempts to predict which *LMNA* variants are pathogenic and to understand their physiological effects lags behind variant discovery. We created *Caenorhabditis elegans* models for striated muscle laminopathies by introducing pathogenic human *LMNA* variants and variants of unknown significance at conserved residues within the *lmn-1* gene. Severe missense variants reduced fertility and/or motility in *C. elegans*. Nuclear morphology defects were evident in the hypodermal nuclei of many lamin variant strains, indicating a loss of nuclear envelope integrity. Phenotypic severity varied within the two classes of missense mutations involved in striated muscle disease, but overall, variants associated with both skeletal and cardiac muscle defects in humans lead to more severe phenotypes in our model than variants predicted to disrupt cardiac function alone. We also identified a separation of function allele, *lmn-1(R204W)*, that exhibited normal viability and swimming behavior but had a severe nuclear migration defect. Thus, we established *C. elegans* avatars for striated muscle laminopathies and identified *LMNA* variants that offer insight into lamin mechanisms during normal development.

Author summary

Muscular dystrophy is a progressive muscle-wasting disorder that eventually leads to cardiac disease. Mutations in the *LMNA* gene, which encodes an intermediate filament protein involved in the structure and organization of the nucleus, is a common but poorly understood cause of this disease. How variants across the breadth of *LMNA* contribute to mechanistic cellular defects that lead to disease is poorly understood, leading to hurdles in diagnosing disease and developing treatments. We found that by introducing amino acid substitutions found in patients with striated muscle disorders caused by *LMNA* into the conserved *lmn-1* gene of the nematode *C. elegans*, we could rapidly test the function of these variants to better understand

their roles. We found that variants modeling diseases that involve both skeletal and cardiac muscle in humans were the most pathogenic in *C. elegans*, typically affecting both viability and movement, while those that modeled cardiac disease alone had less deleterious effects in *C. elegans*. Furthermore, we uncovered molecular mechanisms for how lamins interact with other nuclear envelope proteins to carry out their cellular functions. Thus, our new *C. elegans* models can be used to diagnose and predict the severity of new variants of human *LMNA* as well as better understanding the molecular mechanisms of lamins in normal development.

Introduction

Lamins are highly conserved intermediate filament proteins that underlie the inner nuclear membrane of the nuclear envelope and form a nucleoskeletal meshwork known as the nuclear lamina [1]. Lamins are integral to the mechanical stability of the nucleus, cytoskeletal coupling, genome organization, and gene expression [2]. Pathogenic variants of the human *LMNA* gene contribute to a broad spectrum of tissue-specific diseases that are collectively referred to as laminopathies [3,4]. 80% of pathogenic mutations in *LMNA* give rise to striated muscle laminopathies [5].

Striated muscle laminopathies lead to dilated cardiomyopathy (DCM-CD), which is the main cause of death in affected individuals [3]. However, the range and severity of symptoms within any given *LMNA*-associated striated muscle disease varies [5–7]. While many individuals only have cardiac defects [8], others additionally experience impaired skeletal muscle function [9,10]. At the severe end of the spectrum, *LMNA*-related congenital muscular dystrophy (L-CMD) presents as early onset dystrophic symptoms and rapid disease progression [9,11]. Autosomal-dominant Emery-Dreifuss muscular dystrophy (AD-EDMD) is characterized by childhood onset and manifests as gradual progressive skeletal muscle weakness [6,12]. In contrast, limb-girdle muscular dystrophy type 1B (LGMD1B) is a primarily adult-onset disease with milder weakness typically affecting proximal muscle [13]. How mutations within *LMNA* lead to multiple diseases with a wide range of overlapping etiologies is poorly understood.

Striated muscle laminopathies lack a clear phenotype-genotype link, which further complicates prognoses. The location of a disease-associated variant within the *LMNA* gene does not correspond to symptom onset, type, or severity [14,15]. The need for precise characterization of known pathogenic *LMNA* mutations is compounded by the accelerated pace of variant discovery, which has identified hundreds of variants of unknown clinical significance (VUS), most commonly missense variants [16]. Therefore, a model that can efficiently evaluate the pathogenicity of specific variants is critical to accelerate the diagnosis of *LMNA* VUS. Furthermore, new models would expand our understanding of both the physiological progression of laminopathies and basic roles of lamins throughout normal development.

Vertebrate models have been developed to study the effects of several laminopathic variants. Zebrafish containing a 5-bp deletion that is predicted to create an early stop codon in one or both copies of *lmna* have skeletal muscle defects, reduced movement, and aberrant expression of genes that are also dysregulated in laminopathy patients [17]. $Lmna^{-/-}$ mice lose nuclear envelope integrity, have delayed postnatal growth, and experience a rapid onset of muscular dystrophy, while $Lmna^{+/-}$ mice develop adult-onset DCM [18]. Murine models also exist for laminopathic missense mutations. A line designed to model AD-EDMD with the $Lmna^{L530P/L530P}$ mutation produces mice with symptoms similar to premature aging disorders [19]. Another mouse model, $Lmna^{H222P/H222P}$, develops the dystrophic and cardiac phenotypes of AD-EDMD [20,21]. Notwithstanding these advances, vertebrate models are time-consuming and expensive to generate, limiting their ability to encompass the spectrum of *LMNA*-associated striated muscle laminopathies.

The model nematode *Caenorhabditis elegans* is genetically and microscopically tractable, making it suitable for quickly generating and characterizing mutant strains and an excellent system for studying striated muscle laminopathies. *C. elegans* has a single lamin protein, LMN-1 that is 30.3% identical to human lamin A and performs many of the same functions. LMN-1 binds BAF, emerin, and other LEM-domain homologs, and knock-down of *lmn-1* leads to defects in nuclear shape, chromosome segregation, nuclear import, germline organization, and embryonic viability [22–29]. Because many of the residues in human lamin A that are implicated in disease are conserved in LMN-1, *C. elegans* has been used to model

laminopathy-associated missense variants, and these animals exhibit phenotypes such as defects in striated body-wall muscles that are reminiscent of human pathologies [30–34].

Despite these important advantages, *C. elegans* models to date have been limited in their ability to recapitulate human laminopathies. First, published models express missense variant LMN-1 proteins from multi-copy extrachromosomal arrays in the presence of the intact endogenous *lmn-1* locus [30–34]. Consequently, the relative levels of mutant and wild-type LMN-1 are difficult to accurately measure and may vary from tissue to tissue or cell to cell. Second, most models fuse LMN-1 to fluorescent proteins or tags that have been demonstrated to disrupt lamin function *in vivo* [30,33,35].

Our goal is to characterize laminopathy-associated missense variants of human *LMNA* in order to accelerate phenotypic evaluation of known pathogenic variants and emergent VUS. We established new models that express missense variant proteins from the endogenous *C. elegans lmn-1* locus to better model human disease. We selected *lmn-1* mutations that are homologous to *LMNA* missense variants reported in striated muscle laminopathy patients and classified them based on whether they were known to exhibit cardiac defects only (DCM-CD), or both cardiac and skeletal muscle defects (AD-EDMD). We also evaluated four *LMNA* VUS to determine their potential pathogenicity. To functionally characterize lamin variants, we assayed animal viability and motility. Lamins also interact with components of the LINC complex, which is required to move nuclei during cell migration and has been implicated in striated muscle disorders. We therefore quantified nuclear migration and morphology in hypodermal tissue, revealing new mechanistic insights into lamin function during nuclear migration in normal development.

Results

Introduction of human *LMNA* variants linked to skeletal and cardiac muscle laminopathies into *C. elegans lmn-1*

Our goal was to take clinical *LMNA* variants and edit them into the *C. elegans lmn-1* gene. We selected eight missense variants throughout the open reading frame of human *LMNA* that are linked to diseases that affect skeletal and/or cardiac muscle (Fig 1A). The diseases associated with each selected missense variant are listed in Fig 1A. Three mutations in human *LMNA* (p.E82K, p.E161K, and p.R190W, corresponding to E96K, E175K, and R204W in *C. elegans lmn-1*, respectively) cause defects primarily in cardiac muscle [36–51]. Five variants in human *LMNA* (p.N39S, p.Y45C, p.R50P, p.E358K and p.L530P, equivalent to N53S, Y59C, R64P, E358K, and L535P in *lmn-1*), are associated with earlier age of symptom onset and often are considered more severe, as they contribute to diseases that affect both cardiac and skeletal muscles (red throughout the figures) [6,9,10,12,14,52–58].

A.

Human *LMNA*	# of mutated subjects in UMD/*LMNA*	Families in UMD/*LMNA*	Type of clinical presentation	*C. elegans lmn-1*
N39S	17	17	9 L-CMD, 7 EDMD, 1 LGMD1B	N53S
Y45C	4	4	2 EDMD, 1 DCM-CD, 1 SML	Y59C
R50P	3	3	2 L-CMD, 1 EDMD	R64P
E82K	22	3	12 DCM-CD (in 3 families), 10 asymptomatic (in 2 families)	E96K
E161K	37	18	29 DCM-CD (in 18 families), 8 asymptomatic (in 7 families)	E175K
R190W	75	20	50 DCM-CD (in 20 families), 23 asymptomatic (in 10 families), 2 unknown (in 1 family)	R204W
K270Q	1		1 DCM-CD	K284Q
R331Q	9	9	8 DCM-CD, 1 SML	K331Q
E358K	32	30	11 L-CMD (in 10 families), 19 EDMD (in 18 families), 1 LGMD1B, 1 unknown	E358K
S407D	0		None	G407D
G523R	3	3	1 LGMD1B, 2 DCM-CD	G528R
L530P	3	1	3 EDMD	L535P

B.

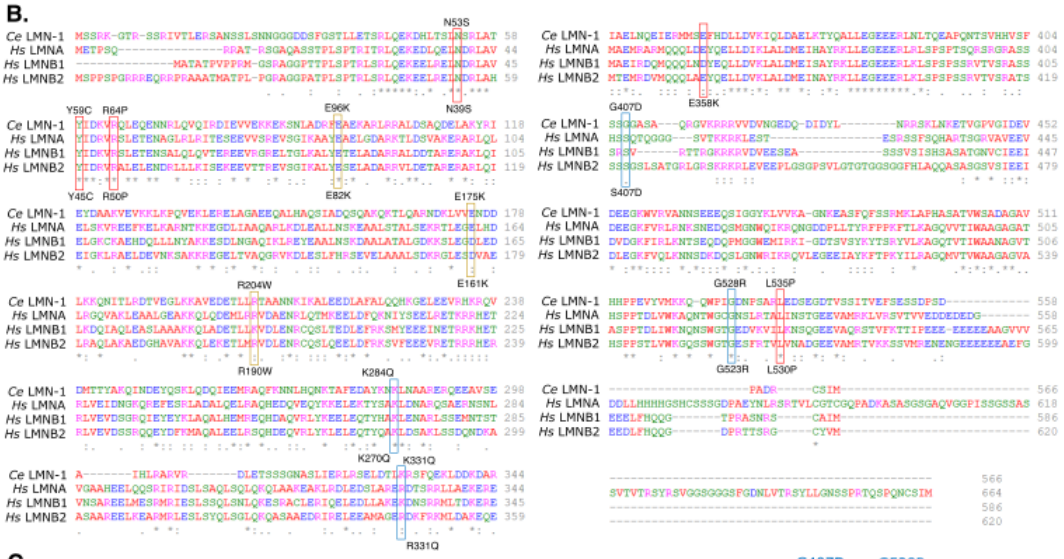

C.

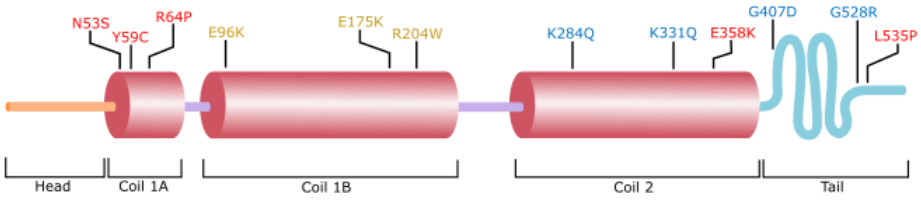

131

132 **Figure 1. Introducing Human *LMNA* Missense Variants into *C. elegans lmn-1*.**

133 (A) Table of human *LMNA* missense variants and the homologous *C. elegans* LMN-1 residue changes. Variants
134 are colored according to their clinical classification: missense variants that exhibit both cardiac and skeletal
135 muscle defects in humans (red), variants that affect cardiac muscle specifically (yellow), and VUS (blue).
136 Clinical presentations and the number of subjects reported are from www.umd.be/LMNA/ (and G Bonne, R
137 Ben Yaou personal communication). L-CMD: *LMNA*-related congenital muscular dystrophy, EDMD: Emery-
138 Dreifuss muscular dystrophy, LGMD1B: limb-girdle muscular dystrophy type 1B, DCM-CD: dilated
139 cardiomyopathy with conduction defects, SML: striated muscle laminopathy (subtype undetermined).
140 Asymptomatic subjects are essentially young 'DCM family' members who may have not yet developed cardiac

disease. (B) Alignment of *C. elegans* LMN-1 and human lamin A/C, lamin B1 and lamin B2 proteins generated by Clustal-Omega multiple sequence alignment. The amino acid changes examined in this study are indicated with boxes, colored as in 1A. *C. elegans* residues are listed above the boxes, and the corresponding human residues are shown below. (C) Diagram of the *C. elegans* LMN-1 protein structure with the head (orange), coils (red) and tail (blue) domains indicated. The positions of the amino acid changes featured in this study are shown using the same color scheme as in A.

We also chose missense *LMNA* VUS (p.K270Q, p.R331Q, and p.G523R, corresponding to K284Q, K331Q, and G528R in *lmn-1*, respectively) that are suspected to be involved in disease. *LMNA* p.G523R has a relatively high allele frequency (0.00006), according to the Genome Aggregation Database (gnomAD) [59], and is therefore predicted to be benign. However, the Clinvar database [60] designates p.G523R, as well as two other *LMNA* VUS (p.K270Q and p.R331Q), as potentially pathogenic based on clinical testing, large-scale genomic analyses of patient cohorts, and *in silico* structural predictions (Fig 1A) [14,49,61–67]. The fourth VUS, *LMNA* p.S407D, which corresponds to *lmn-1(G407D)*, is a predicted benign variant that has not previously been associated with disease [68].

We generated homologous missense variants of *C. elegans lmn-1* corresponding to each of the eight pathogenic *LMNA* variants and the four VUS (Fig 1). Homozygous point mutations were engineered into the endogenous *lmn-1* locus using CRISPR-Cas9-mediated genome editing. We will refer to the variants using the amino acid position in the *C. elegans* LMN-1 protein throughout the rest of this manuscript.

lmn-1 variants that model skeletal and cardiac muscle disorders exhibit reduced fitness

lmn-1 (RNAi) causes embryonic lethality [24]. Chromosome segregation defects are evident as early as the 2-cell stage, and embryos arrest around the 100-cell stage, indicating that *lmn-1* is required for early embryonic development [24]. Although *lmn-1* null homozygous animals from heterozygous mothers are able to develop with the help of maternally-loaded LMN-1, they are sterile due to the lack of lamin in the

germline [69]. We therefore examined the effect of the *lmn-1* missense mutations on overall *C. elegans* health and fitness by quantifying the brood size and level of embryonic lethality of each engineered line.

All five *C. elegans* strains carrying missense *lmn-1* mutations that model human *LMNA* variants associated with both skeletal and cardiac muscle dysfunction had significant viability and fertility defects (Fig 2). Homozygous N53S, Y59C, R64P, and L535P LMN-1 variants had the most deleterious effects on brood size. These strains were maintained as balanced heterozygotes. Homozygous animals from heterozygous mothers survived to adulthood, which allowed us to assay the effect of having no genetically-encoded wild-type copies of *lmn-1*. Homozygous L535P adults were sterile, failing to lay any eggs. N53S homozygous animals laid some eggs, but none were viable. LMN-1 Y59C and R64P homozygous animals had small broods, roughly 30-40% the size of those of wild type animals. In addition, embryonic lethality in Y59C and R64P animals was 20-30% higher than that of wild type. E358K also had a significantly reduced brood size, less than 40% that of wild type. Half of E358K animals laid few or no embryos and had elevated lethality.

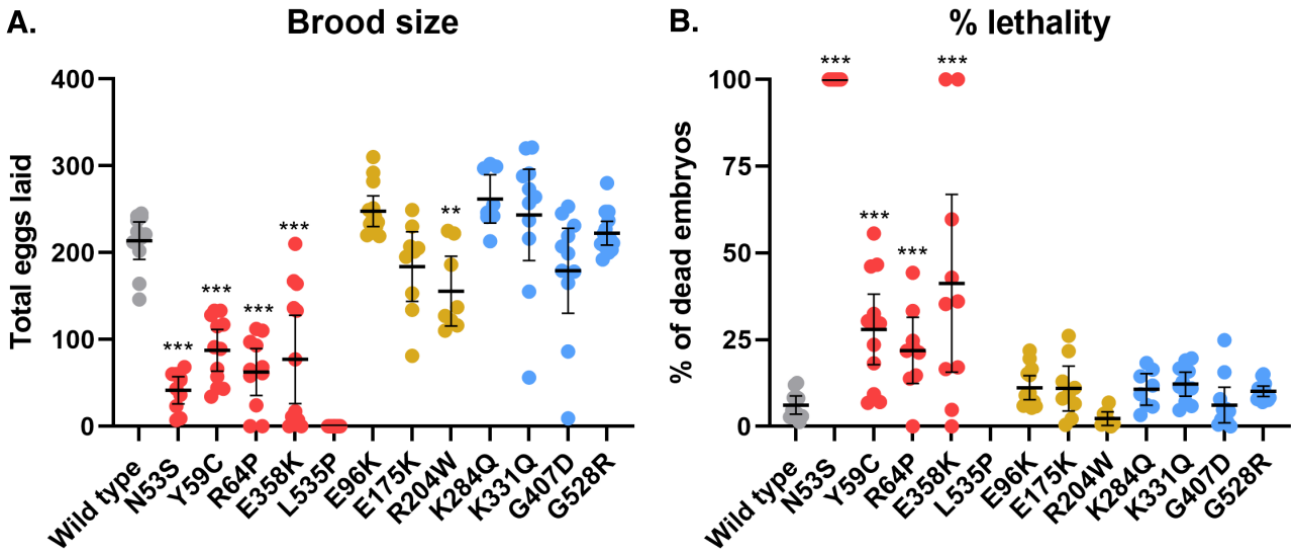

Figure 2. Severe Human Pathogenic *LMNA* Variants Modeled in *C. elegans lmn-1* Cause Decreased Brood Size and Elevated Embryonic Lethality. (A) Brood size of wild type and *lmn-1* homozygous missense mutant lines. Each dot represents the average number of eggs laid by a single animal. (B) The percent of

182 embryos laid that failed to hatch within 24 hours for each genotype is shown. Each dot represents the average
183 number of eggs laid by a single animal. Both A and B are grouped and colored according to clinical
184 classifications as in Fig 1. n = 8-12 animals. Means and 95% CI are shown. Significance compared to wild type
185 was calculated using student's t test. **p≤0.01; ***p≤0.001.

186 In contrast to the mutants modeling diseases affecting both skeletal and cardiac muscles, *lmn-1* mutants
187 modeling *LMNA* variants associated solely with DCM-CD (E96K, E175K, and R204W), did not show
188 pronounced reductions in brood size or heightened lethality. Likewise, the four VUS showed no defects in
189 viability or fertility compared to wild type animals. These results indicate that our *C. elegans* models reflect
190 how missense variants linked to muscle and cardiac laminopathies like L-CMD and EDMD in humans
191 reduce overall health and fitness.

192 Most *lmn-1* missense mutants had impaired swimming behavior

193 Muscular dystrophies usually manifest as defects in skeletal muscle function that variously restrict mobility
194 [5]. We therefore assayed swimming behavior [31,70] in our *lmn-1* variant lines to test whether
195 physiological changes in *C. elegans* might predict the potential severity of *LMNA*-associated striated muscle
196 disease missense variants. We assayed major motor movements by observing animals thrashing in buffer
197 and quantified the number of body bends per second (BBPS) for each of the homozygous missense lines
198 (Fig 3). We also measured swimming in heterozygous animals carrying variants that caused major viability
199 and fertility defects.

200 LMN-1 L535P homozygous animals had the most severe motility defects, averaging less than 1 BBPS,
201 followed by LMN-1 Y59C with a rate of 1.1 BBPS compared to 1.86 BBPS in wild type (Fig 3B). However,
202 we observed a wide distribution of phenotypes within each strain, with individual animals exhibiting
203 anywhere from normal swimming behavior to severely reduced or undetectable movement. To test the
204 significance of the effect of *lmn-1* missense mutations on motility, we scored the percentage of individuals

in each strain that thrashed more slowly than the mean rate of *lmn-1(Y59C)*, which at 1.1 BBPS is a well-studied mutation in *C. elegans* known to disrupt swimming (Fig 3C) [30,31,70].

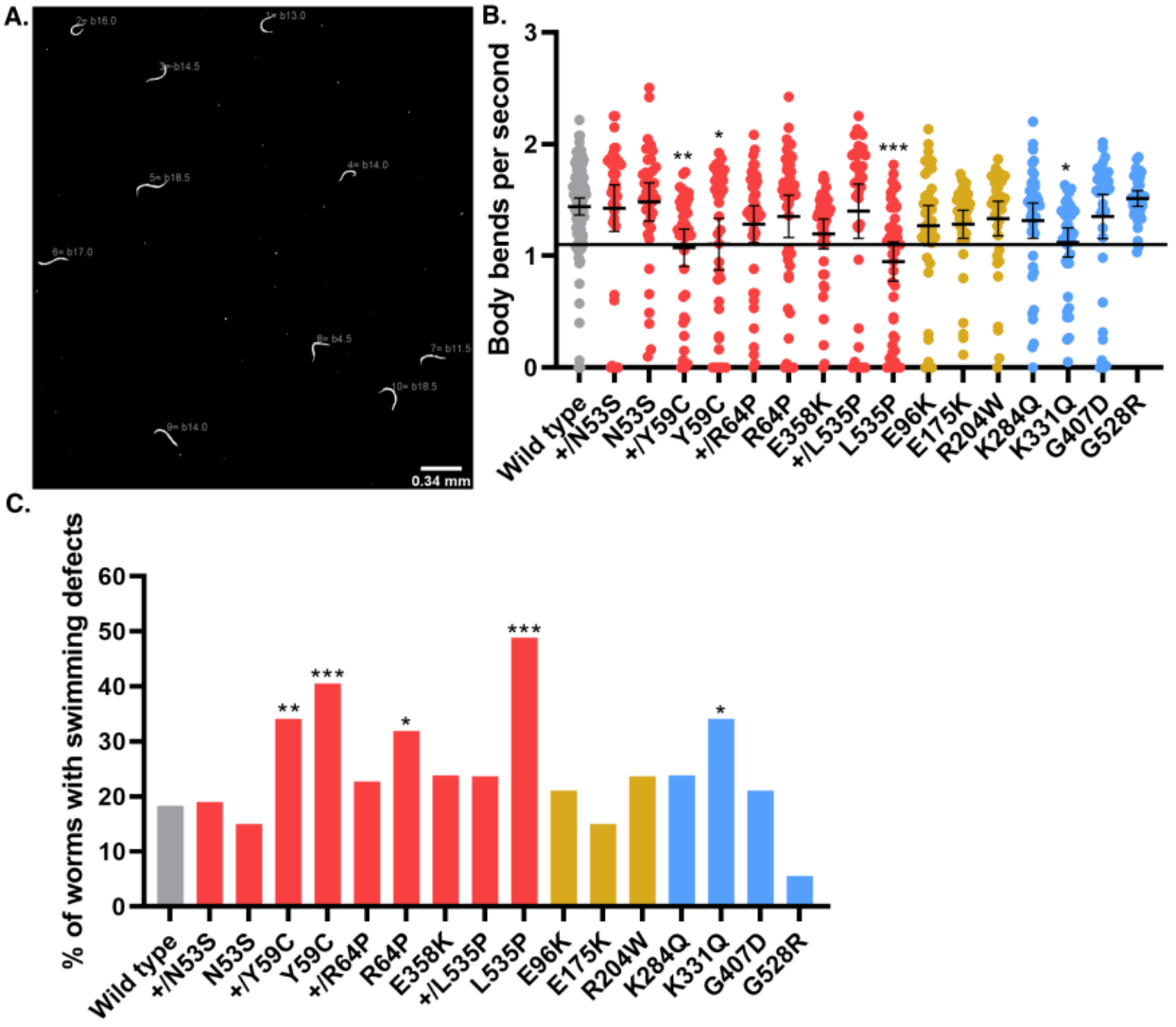

Figure 3. *lmn-1* Missense Variants can Reduce Swimming Motility. (A) An example of a processed swimming video. Each animal is assigned a number by the Fiji wrMTrck plugin, which records the number of body bends per second (BBPS) (shown in dark gray beside the animals). (B) Each dot represents a single animal that was tracked over 30 seconds. BBPS over the 30 second interval is shown. Genotypes (homozygous (e.g., N53S) and heterozygous (e.g., N53S/+)) are grouped by variant clinical classification as in Fig 1. Significance was calculated using a one-way ANOVA and corrected for multiple comparisons using Dunnett's test. *p≤0.05; **p≤0.01; ***p≤0.001 A threshold of 1.1 BBPS is indicated by the line. Means and error bars of 95% CI are

shown. n ~ 40 animals, except for wild type which is ~100. (C) The same data as in B, but instead, the bars represent the percentage of animals with swimming defects below 1.1 BBPS for each strain. Significance was determined by chi-squared test of the percentage of individuals in each strain that fell at or below 1.1 BBPS as compared to wild type. *p≤0.05; **p≤0.01; ***p≤0.001.

Four homozygous *lmn-1* mutations (Y59C, R64P, K331Q and L535P) caused severe swimming defects. Three of these mutations (Y59C, R64P, and L535P) were designed to model human mutations in *LMNA* that affect both skeletal and cardiac muscle function. Of the alleles that were designed to model cardiomyopathy-linked variants without skeletal muscle involvement (Fig 3), none caused significant motility defects. Three of the VUS, K284Q, G407D, and G528R, had normal swimming rates (Figs 3B-C). In contrast, K331Q had a statistically significant swimming defect, suggesting this VUS is pathogenic. Since our initial test, K331 was linked to DCM-CD (Table1), validating our approach for predicting VUS pathogenicity.

A cardiomyopathy-linked missense variant drastically disrupts nuclear migration

Knocking down *lmn-1* via RNAi leads to embryonic lethality [24]. However, animals that survive due to a presumably low level of RNAi have nuclear migration defects in embryonic dorsal hyp7 precursor cells [71]. Hyp7 precursor nuclei that fail to migrate are mislocalized in the dorsal cord of *lmn-1(RNAi)* early larval stage animals, suggesting that LMN-1 is required for this migration event (Fig 4A). Therefore, we examined the extent to which our *lmn-1* missense mutations might affect nuclear migration. We used a previously described line expressing a nuclear GFP marker specifically in the hypodermis to assay nuclear migration in hyp7 precursor cells [72]. *lmn-1(N53S)* and *lmn-1(Y59C)* homozygous animals had significant nuclear migration defects, where 20-35% of hyp7 nuclei were mislocalized in the dorsal cord (Figs 4B and C). Interestingly, R204W displayed a severe hyp7 nuclear migration defect, where about 75% of hyp7 precursor nuclei failed to migrate (Figs 4B and C). None of the other missense mutant lines, including the

VUS, significantly disrupted nuclear migration. These data suggest that residues N53 and Y59 contribute to the function of LMN-1 in nuclear migration while R204 is critical to the role of LMN-1 during nuclear migration in the developing hypodermis.

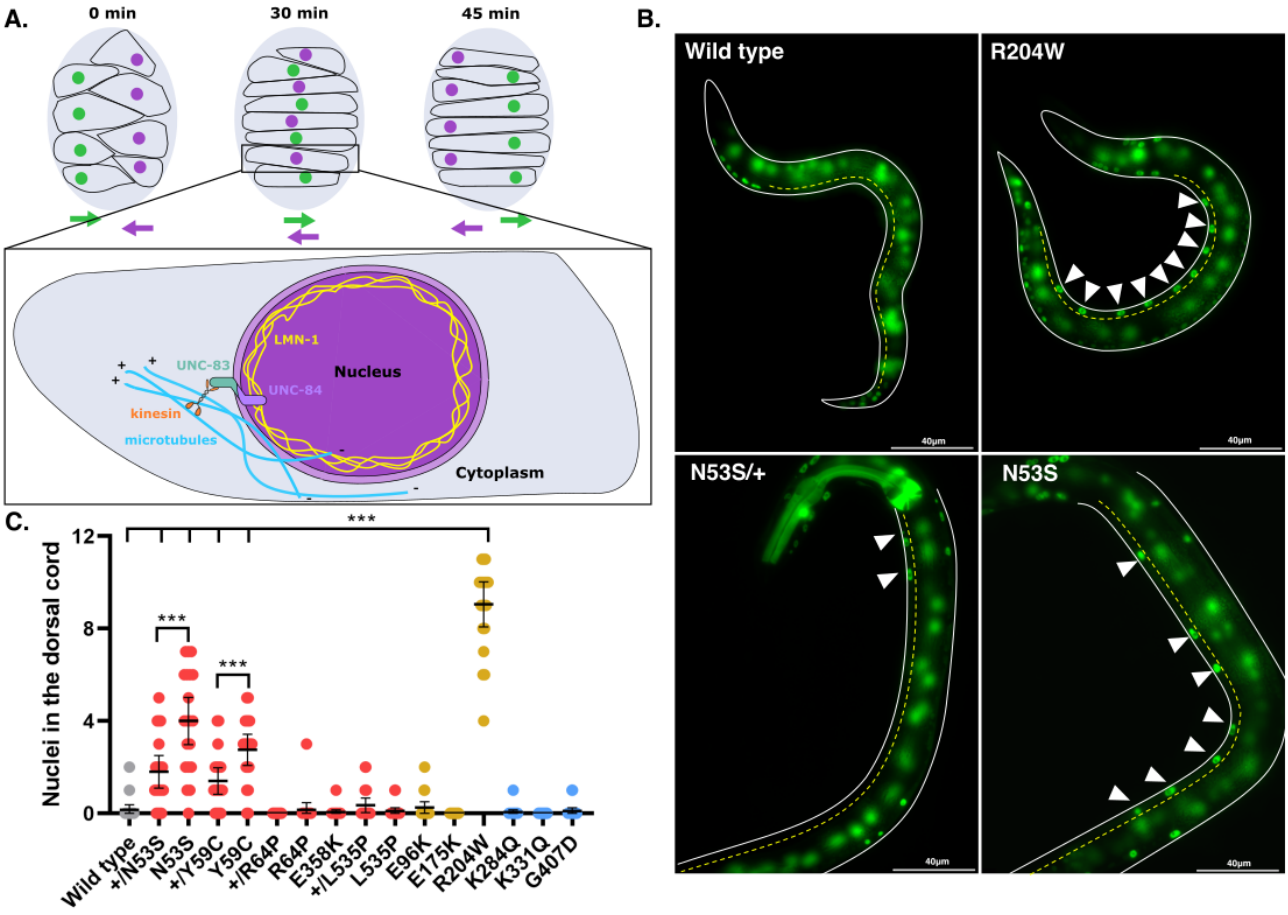

Figure 4. *lmn-1* Missense Variants can Lead to Defects in Nuclear Migration. (A) Schematic of nuclear migration in hypodermal cells. Dorsal hyp7 precursor nuclei (purple and green circles) migrate to opposite sides of the embryo (gray; dorsal view; anterior is up) over the course of ~45 minutes. Colored arrows show the direction of migrating nuclei of the same color. Inset shows the molecular motor kinesin (orange) attached to the LINC complex, made up of UNC-83 and UNC-84 (teal and violet, respectively), which binds to lamin (yellow) and facilitates nuclear migration in hyp7 precursors. Microtubules (blue) are shown with their plus ends in front of the migrating nucleus. (B) Representative epifluorescence images of animals with the indicated genotypes expressing a GFP nuclear marker in hyp7 cells. GFP fluorescence in the pharynx of N53S/+ marks the presence of the balancer chromosome. On the left is the dorsal cord, (yellow dotted line), and the ventral

side of the animal is shown on the right. Arrowheads indicate mislocalized nuclei in the dorsal cord. Scale bar: 40µm. (C) Number of nuclei mislocalized in the dorsal cord of wild type and missense variant lines. Each dot represents a single worm. n=20 per genotype. Means and 95% CI are shown. ***p≤0.001.

LMN-1 directly interacts with the nucleoplasmic domain of the inner nuclear membrane SUN (Sad1/UNC-84) protein UNC-84, and is necessary for the assembly of the Linker of the Nucleoskeleton and Cytoskeleton (LINC) complex [71]. Once UNC-84 is recruited to the inner nuclear membrane, it recruits the KASH (Klarsicht/ANC-1/SYNE homology) protein UNC-83 to the outer nuclear membrane, and the binding of both proteins in the perinuclear space forms the nucleo-cytoskeletal bridge known as the LINC complex [73]. To determine whether the *lmn-1(R204W)* variant disrupts the interaction between the LINC complex and LMN-1, we examined the nuclear envelope localization of UNC-83 and UNC-84. In the *lmn-1(R204W)* background, the intensity of UNC-83 immunofluorescence was significantly lower than that of wild type in embryonic hyp7 precursor nuclei (Figs 5A and B). Similarly, we observed reduced fluorescence intensity of GFP-tagged UNC-84 at the nuclear envelope in the hypodermis of R204W compared to wild-type young adult animals (Fig 5C). Together, these data suggest that the LMN-1 R204W variant interferes with the formation of the LINC complex by disrupting UNC-84 and UNC-83 localization to the nuclear envelope in the *C. elegans* hypodermis.

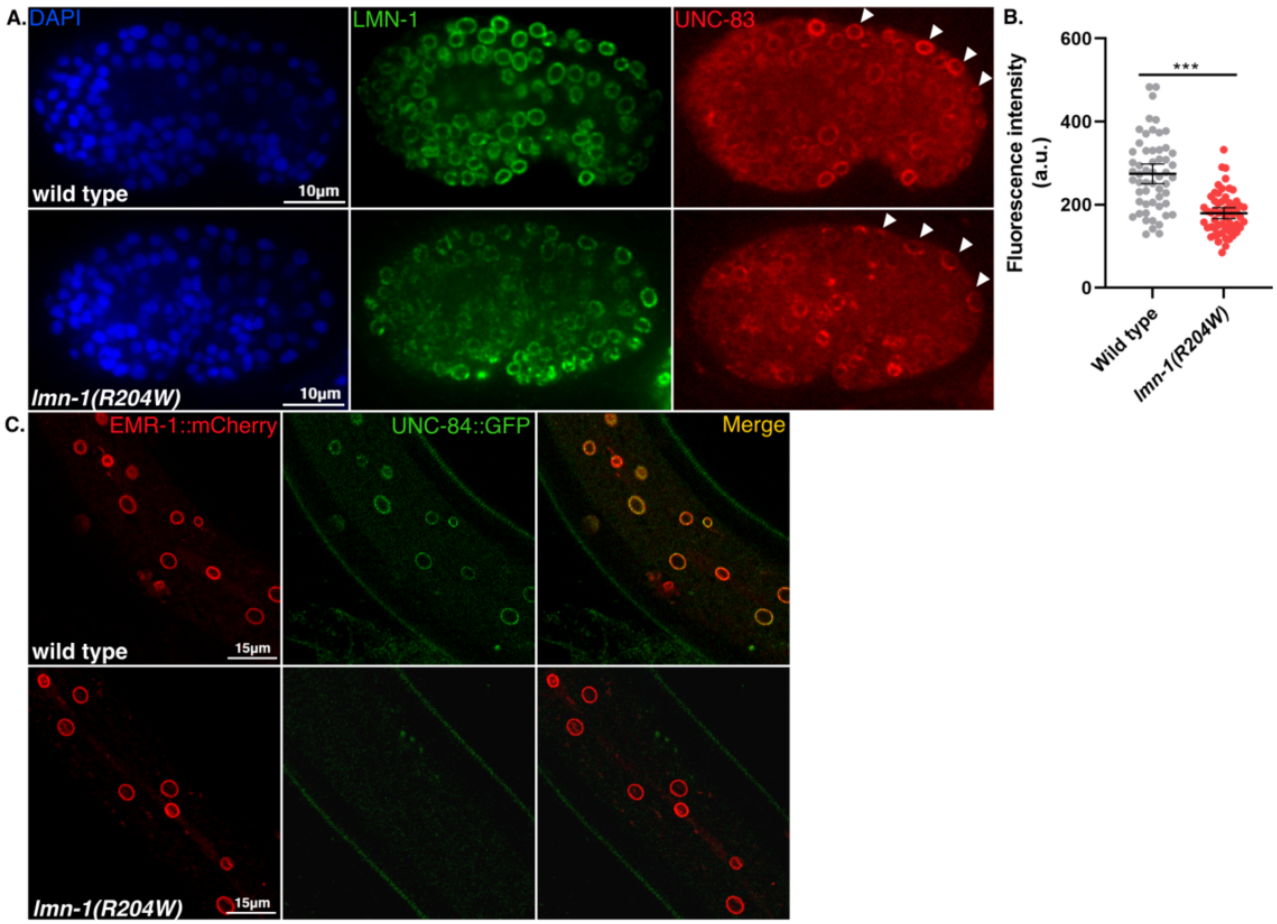

Figure 5. The *lmn-1(R204W)* Missense Variant Disrupts UNC-84 and UNC-83 Localization to the Nuclear Envelope. (A) Immunofluorescence images showing anti-UNC-83 localization to the nuclear periphery of dorsal hypodermal nuclei (white arrowheads) in wild-type and *lmn-1(R204W)* comma-stage embryos. Anti-LMN-1 immunostaining (green) and DAPI-stained nuclei (blue) are also shown. Scale bar: 10µm (B) Fluorescence intensity (arbitrary units) of UNC-83 at the nuclear envelope of wild type embryos (n=10, 56 nuclei) and *lmn-1(R204W)* embryos (n=12, 57 nuclei). Means and error bars of 95% CI are shown. Significance was calculated using student's t test. ***= $p<0.001$. (C) Representative confocal images of EMR-1::mCherry and UNC-84::GFP-tagged hypodermal nuclei in live wild type and *lmn-1(R204W)* young adult animals. Scale bar: 15µm.

Some *lmn-1* variants have abnormal nuclear morphology and high numbers of micronuclei

Disrupting A-type nuclear lamins in mammalian or invertebrate models leads to nuclear blebbing, chromosome bridges, and the formation of micronuclei [24,74–77]. We assayed nuclear morphology in *C. elegans* hypodermal syncytia to determine the extent to which missense mutations in *lmn-1* affect nuclear architecture and stability.

We screened for abnormal nuclear morphology in the hyp7 syncytia of young adults using a nuclear GFP marker expressed in the hypodermis [72]. Three *lmn-1* variant strains (N53S, Y59C, and L535P) had severe nuclear morphology defects, including misshapen and lobulated nuclei, chromatin bridges, and micronuclei (Fig 6A). To quantify these defects, we focused on the number of micronuclei present in each animal. N53S, Y59C, and L535P animals had the highest number of micronuclei. Strains with the other two variants designed to model both skeletal and cardiac pathologies (R64P and E358K) had fewer micronuclei, but statistically more than wild type (Fig 6B). R204W, K284Q, and K331Q variant strains also had mild, but statistically significant, micronuclear defects. The evidence that missense mutations in *lmn-1* can cause defects in nuclear envelope morphology and the formation of micronuclei indicates that nuclear instability may play a role in the pathology of striated muscle laminopathies.

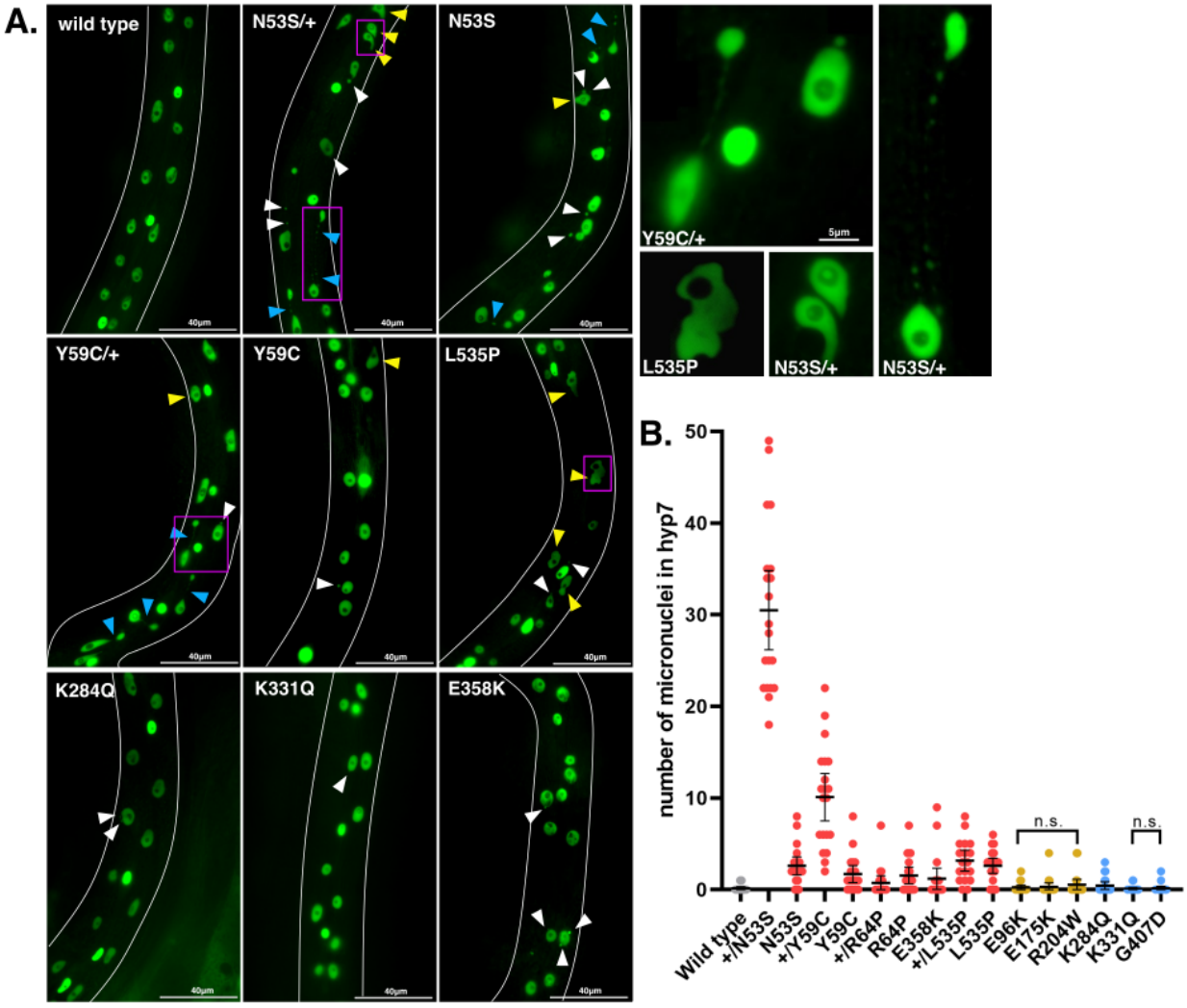

Figure 6. Missense Mutations in *lmn-1* Often Result in Abnormal Hypodermal Nuclear Morphology and the Formation of Micronuclei. (A) Representative epifluorescence images of animals with the indicated genotypes expressing a GFP nuclear marker in hyp7 cells. Micronuclei (white arrowheads), blebbed nuclei (yellow arrowheads), and chromosome bridges (blue arrowheads) are indicated. Scale bar: 40µm. Magenta boxes designate nuclei featured in the insets on the right. Scale bar: 5µm. (B) Number of micronuclei on one lateral side of the hyp7 syncytia in a young adult. The genotypes are colored as in Fig 1. n = 20. Means and error bars of 95% CI are shown. To control for type 1 error, p values were adjusted using the Benjamini-Hochberg procedure with a false discovery rate of 5%.

Discussion

Mutations in *LMNA* give rise to a host of diseases that affect striated muscle, which lead to dilated cardiomyopathy that may or may not be associated with skeletal muscle defects. However, symptom onset, type, and severity overlap across striated muscle laminopathies and range widely within each. Furthermore, causative *LMNA* missense variants are not exclusive to specific diseases or domains of the protein, and their effects on lamin structure and function are unclear [15]. The vast majority of known pathogenic *LMNA* mutations are missense variants, and many other variants remain uncharacterized or have conflicting evidence for pathogenicity. Here we establish a pipeline to rapidly generate models of clinical VUS using gene-edited versions of *C. elegans lmn-1*. We found that by subjecting the *C. elegans lmn-1* variant strains to a series of cellular and physiological assays, we could discern the degree of severity of different disease-causing human *LMNA* variants and assess the likelihood of VUS to contribute to disease. The modeled missense mutations also uncovered new mechanistic insights into the normal roles of lamin in development. Our assays yielded a broad distribution of phenotypic severity within each *lmn-1* missense variant population, reflective of the wide range of symptom severity observed in human laminopathies. Previous *C. elegans* models show similar results, where animals expressing extra copies of GFP-tagged LMN-1 Y59C or LMN-1 L535P in an otherwise wild-type LMN-1 background have variously impaired movements [30,78]. Our data suggest that viability and motility are primary indicators of variant pathogenicity, followed by micronuclei formation and nuclear migration defects. We established a scoring system which incorporates cellular and physiological defects in the *C. elegans* models to predict the potential pathogenicity of each variant (Table 1). Variant strains that were homozygous inviable scored two, and those with significantly reduced viability compared to wild type scored one. Variant strains where greater than 30% of the animals had swimming defects scored two, while strains in which less than 30% of animals exhibited swimming defects were scored zero. Finally, a score of one was assigned to strains with nuclear migration defects. By this metric (Table 1), we found that our models reflect the distinction between severe *LMNA* mutations that affect both cardiac and skeletal muscle (score ≥ 2), and those that tend to contribute

to cardiac defects alone (score <2). These scores correlate with the frequency that these variants are found in humans (Fig 1A). Childhood-onset *LMNA* variants are rare in comparison to adult-onset pathologies that are more likely to be passed through families. Finally, our scoring system predicts that one *LMNA* VUS (p.R331Q) is pathogenic, while the others (p.K270Q, p.S407D, and p.G523R) are unlikely to contribute to disease.

Table 1. Phenotypic Scoring of *C. elegans* Laminopathy Models.

Human *LMNA*	*C. elegans lmn-1*	Viability*	Swimming†	Nuclear migration§	Score
N39S	N53S	2	0	1	3
Y45C	Y59C	1	2	1	4
R50P	R64P	1	2	0	3
E358K	E358K	1	0	0	1
L530P	L535P	2	2	0	4
E82K	E96K	0	0	0	0
E161K	E175K	0	0	0	0
R190W	R204W	0	0	1	1
K270Q	K284Q	0	0	0	0
R331Q	K331Q	0	2	0	2
S407D	G407D	0	0	0	0
G523R	G528R	0	0	N/A	0

*Score 2 for homozygous inviable, 1 for decreased viability, and 0 for wild type

†Score 2 when >30% of animals show a severe defect, and 0 when <30% of animals have severe defects

§Score 1 for defective nuclear migration and 0 for wild type

Human striated muscle laminopathies are primarily dominant disorders [7]. We therefore included heterozygous animals in our analyses of severe *lmn-1* mutations that model both cardiac and skeletal defects (N53S, Y59C, R64P and L535P). These lines largely acted in a dominant fashion in our assays. Furthermore, N53S/+ and Y59C/+ animals had the most severe micronuclei phenotypes, even in comparison to their homozygous counterparts (Fig 6B). Higher numbers of micronuclei in heterozygous

350 animals may result from a dominant-negative effect of wild-type LMN-1, as is hypothesized to occur in
351 human *LMNA*-associated pathologies [16,79]. Similar nuclear morphology defects were observed in
352 heterozygous and homozygous N53S, Y59C, and L535P *lmn-1* hypodermal nuclei, indicating a general loss
353 of the nuclear structure integrity.

354 Nuclear instability can be a hallmark of striated muscle disease [80]. The formation of micronuclei may
355 originate from errors in chromosome segregation, as has been previously described in *lmn-1(RNAi)* early
356 embryos [24]. This idea is supported by decreased fertility in these *lmn-1* missense variant strains.
357 Alternatively, human laminopathies that affect both skeletal and cardiac muscle often have dysmorphic
358 nuclei, which are proposed to be the result of the extreme mechanical forces these nuclei are subject to [81–
359 83]. A third possibility is that nuclear deformation could result from altered nucleocyto-skeletal coupling
360 in *lmn-1* missense variants, similar to what has been reported in other laminopathy models [30,84,85].

361 Lamins directly bind to LINC complexes through the nucleoplasmic domains of SUN proteins at the inner
362 nuclear membrane [71,86]. LINC complex components have been implicated in DCM-CD and EDMD, but
363 the mechanisms by which LINC interfaces with lamins and how defects in this interaction contribute to
364 disease are poorly understood [15]. We found that cardiomyopathy-associated *lmn-1(R204W)* variant
365 animals exhibited a strong nuclear migration defect but did not have defects in viability or motility.
366 Furthermore, LINC complex components failed to localize to the nuclear envelope in *lmn-1(R204W)*
367 animals. Thus, we have isolated a separation-of-function allele that does not disrupt the global function of
368 lamins. Instead, our data are consistent with a hypothesis that *lmn-1(R204W)* specifically disrupts the
369 physical interaction between lamins and the LINC complex. This allele will be valuable for future
370 experiments studying the role of LINC complexes in laminopathies and suggests that a potential mode of
371 pathogenicity in R204W variant animals is through disruption of the interaction between SUN and LMN-
372 1.

373 In summary, our data provides a blueprint for creating and evaluating *C. elegans* clinical avatars for
374 laminopathy-associated missense variants of human *LMNA* and new models to understand the mechanisms

of lamin function during normal development. We created molecular and physiological assays for identifying potentially pathogenic missense variants and used these indicators to develop a scoring index in our *C. elegans* models that can be used to predict the tissues affected and relative rate of disease progression in humans with orthologous variants. Furthermore, we identified a separation-of-function point mutation that specifically disrupts the interaction between lamins and LINC complexes. In the future, these new *C. elegans lmn-1* missense variant models could also be used to screen candidate drugs to treat striated muscle laminopathies.

Materials and methods

C. elegans genetics and gene editing

Strains were grown on nematode growth medium (NGM) plates spotted with OP50 *Escherichia coli* and maintained at room temperature (22-23°C) [87]. Strains used in this study are listed in Table 2. Some strains were obtained from the Caenorhabditis Genome Center, which is funded by NIH Office of Research Infrastructure Programs (P40 OD010440).

lmn-1 missense strains were generated using a *dpy-10* co-CRISPR strategy [88–91]. crRNAs and repair template sequences are in Table 2. Injection mixes were made and injected as described previously [92]. Briefly, for UD796, UD750 and UD788 missense strains, an injection mix containing 0.2µL *dpy-10* crRNA (0.6mM from Horizon discovery/Dharmacon), 0.5µL *lmn-1* crRNA (0.6mM), 2.47µL of universal tracrRNA (0.17mM), was combined and added to 7.68µL of purified Cas9 protein (0.04mM from UC Berkeley QB3). The assembly was completed with the addition of 0.28µL of the *dpy-10* single-stranded DNA oligonucleotide (ssODN) (500ng/µL) and 0.21µL of the *lmn-1* ssODN (500ng/µL) repair templates to form CRISPR-Cas9 complexes *in vitro*. For NMX419, NMX554, NMX563, NMX567, NMX589, NMX421, NMX557, and UD837 strains, injection mixes containing 0.8µL *dpy-10* crRNA (30pmol/µl from Synthego Corporation) and 1.65µL of each of two *lmn-1* crRNA per strain (30pmol/µl)

was combined and added to 1µL of purified Cas9 protein (5µg/µl from PNA Bio, Inc). Following addition of 1µL of the *dpy-10* ssODN (500ng/µL) and 1µL of the *lmn-1* ssODN (500ng/µL) repair templates (Integrated DNA Technologies, Inc). Mixes were injected into the gonads of young adult hermaphrodites. Animals were screened for successful edits using PCR primers ods2621 (5'-TGGCTCAACGCTTCTAGAAACTTC-3') and ods2672 (5'- CATGACAACCTACGCCAAGCAG-3').

Physiological and molecular assays

To score brood size, L4 animals were singled onto OP50 *E. coli* NGM plates and left to grow for 42 hours, during which they reach adulthood (18 hours) and lay their first batch of eggs (24 hours). Every 24 hours, worms were transferred to new plates, for a total of three days. The total number of eggs and offspring on the previous plate was counted 24 hours after the animals were moved to new plates. The percent lethality of each strain was found by quantifying the number of unhatched eggs and dividing the sum by the brood size.

To assay swimming motility, 8-10 L4 animals were picked onto an unspotted NGM plate, which was then flooded with M9 buffer and placed on a light microscope equipped with a Samsung Galaxy A51 5G smartphone attached to the eyepiece. Videos were taken with the smartphone's camera at 30fps. Animals were filmed for thirty seconds. Videos were converted to AVI format using ffmpeg and subsequently processed for background subtraction and binarization in Fiji [93]. The number of body bends per second (BBPS), was quantified using the wrMTrck plugin [94].

Nuclear migrations of embryonic hyp7 precursors were scored in larval animals by counting the number of nuclei abnormally localized in the dorsal cord as described previously [72]. To assay nuclear morphology, L4 animals were picked onto plates and allowed to grow for 20 hours. Young adults were then mounted onto 2% agarose pads in ~5µL of 1mM tetramisole in M9 buffer. The number of micronuclei were counted, including those associated with chromosome bridges. Only one lateral side of each animal was scored.

Nuclei were visualized using a wide-field epifluorescent Leica DM6000 microscope with a 63 × Plan Apo 1.40 NA objective, a Leica DC350 FX camera, and Leica LAS AF software.

lmn-1(R204W) immunofluorescence and imaging

Comma-stage wild-type and *lmn-1(R204W)* embryos were fixed and stained with monoclonal antibody 1209D7 against UNC-83c as previously described [73]. The anti-LMN-1 polyclonal guinea pig antibody was used at a dilution of 1:1000 (gift of Jun Kelly Liu, Cornell University) [95]. Fluorescence intensity of dorsal hypodermal nuclei was calculated using the following equation: Corrected total nuclear fluorescence = Integrated density – (Area of each nucleus x Mean fluorescence of the background). The integrated density is the product of the selected area and the average gray value within the selection. Values were found using ImageJ. Confocal images were taken on a Zeiss LSM 980 with Airyscan using a 63x Plan Apo 1.4 NA objective and the Zeiss Zen Blue software made available through the MCB light imaging microscopy core and through NIH grant S10OD026702.

Statistics

Scatter plots show the mean and 95% confidence intervals (CI) as error bars. Swimming phenotypes were analyzed using a chi-squared test comparing the number of wild type animals that fell below a threshold of 1.1 BBPS, which corresponds to the corroborated mean swimming rate of *lmn-1(Y59C)* worms [31,70] to the missense mutant populations. Percentages and their corresponding p values are shown in the bar graph. Unpaired student's t tests were used for nuclear migration and were corrected with Tukey. Nuclear morphology was evaluated using the Benjamini-Hochberg adjusted p value and setting a false discovery rate of 0.05. Graphs were generated with Prism 9 software.

Table 2. Strains Used in this Study.

Strain	Genotype	Reference
N2	wild type	[87]
UD796	*lmn-1(yc107[N53S]) I/hT2 [bli-4(e937) let(q782) qIs48[P_{myo-2}::gfp; P_{pes-10}::gfp; P_{ges-1}::gfp]] (I;III)*	This study
UD750	*lmn-1(yc96[Y59C]) I/hT2 (I;III)*	This study
UD788	*lmn-1(yc105[R64P]) I/hT2 (I;III)*	This study
NMX419	*lmn-1(tgx395[E96K]) I*	This study
NMX554	*lmn-1(tgx526[E175K]) I*	This study
NMX563	*lmn-1(tgx535[R204W]) I*	This study
NMX567	*lmn-1(tgx539[K284Q]) I*	This study
NMX589	*lmn-1(tgx561[K331Q] I*	This study
NMX421	*lmn-1(tgx397[E358K]) I*	This study
NMX414	*lmn-1(tgx390[G407D]) I*	This study
NMX557	*lmn-1(tgx529[G528R]) I*	This study
UD837	*lmn-1(tgx550 [L535P]) I/hT2 (I;III)*	This study
LW905	*lmn-1(tm1502) I/hT2 (I;III)*	[69]
UD398	*him-8(e1489) IV; ycIs10[P_{col-10}::nls::gfp::lacZ] V*	[71]
UD899	*lmn-1(yc107[N53S]) I/ hT2 (I;III); him-8(e1489) IV; ycIs10V*	This study
UD883	*lmn-1(yc96[Y59C]) I/hT2 (I;III); him-8(e1489) IV; ycIs10 V*	This study
UD895	*lmn-1(yc105[R64P]) I/hT2 (I;III); him-8(e1489) IV; ycIs10 V*	This study
UD915	*lmn-1(tgx395[E96K]) I; him-8(e1489) IV; ycIs10 V*	This study
UD913	*lmn-1(tgx526[E175K]) I; him-8(e1489) IV; ycIs10 V*	This study
UD908	*lmn-1(tgx535[R204W]) I; him-8(e1489) IV; ycIs10 V*	This study
UD835	*lmn-1(tgx539[K284Q]) I; him-8(e1489) IV; ycIs10 V*	This study
UD834	*lmn-1(tgx561[K331Q]) I; him-8(e1489) IV; ycIs10 V*	This study
UD839	*lmn-1(tgx[E358K]) I; him-8(e1489) IV; ycIs10 V*	This study
UD836	*lmn-1(tgx390[G407D]) I; him-8(e1489) IV; ycIs10 V*	This study
UD857	*lmn-1(tgx550[L535P]) I/hT2 (I;III); him-8(e1489) IV; ycIs10 V*	This study
BN147	*emr-1(gk119) I; bqSi142 [P_{emr-1}::emr-1::mCherry] II*	[96]
UD453	*unc-84(yc23[unc-84::GFP]) X*	[97]
UD1008	*unc-84(yc23[unc-84::GFP]) X; emr-1(gk119)? I; bqSi142 [P_{emr-1}::emr-1::mCherry] II*	This study
UD1009	*unc-84(yc23[unc-84::GFP]) X; lmn-1(tgx535[R204W]), emr-1(gk119)? I; bqSi142 [P_{emr-1}::emr-1::mCherry] II*	This study

454 **Table 3. crRNA and Repair Templates Used in this Study.**

455

New alleles	Strain	crRNA*	DNA repair template*†§
lmn-1(yc107[N53S]) I/hT2 [bli-4(e937) let(q782) qIs48[P_{myo-2}::gfp; P_{pes-10}::gfp; P_{ges-1}::gfp]] (I;III)	N2	AAAACUCAC GUCGAUGUA AG	GGCTCAACGCTTCTAGAAACTTCACGTCTTCA AGAGAAAGATCATTTGACgTCACTCAgCAGTC GTCTTGCtACTTACATCGACGTGAGTTTTAAT TTGGAAAGTATTCATATTTGA
lmn-1 yc96[Y59C]) I/hT2 (I;III)	N2	AAAACUCAC GUCGAUGUA AG	AAGTGTACTTTCAAATATGAATACTTTCCAAA TTAAAACTCACGTCGATGcAcGTaGCAAGACG ACTGTTGAGTGAAGTCAAATGATCTTTCTCTT GAAGACGTGA
lmn-1(yc105[R64P]) I/hT2 (I;III)	N2	GCAAGAGAA CAACAGACU CC	TTTTAATTTGGAAAGTATTCATATTTGAAAGT ACACTTTTCAGAAAGTTCcTCAAcTGGAGCAA GAGAACAACAGACTCCAaGTTCAAATTCGCGA CATCGAAGTTGTTGAAAAGAAAGAGAAGTCAA ACTT
lmn-1(tgx395[E96K]) I	N2	CGATGTCGC GAATTTGAA CC CGATCGCTT CGAGGCGGA AA	CGTCAATTGGAGCAAGAGAACAACAGACTCCA GGTcCAgATcCGtGAtATtGAgGTcGTcGAgA AaAAgGAaAAaTCtAAtTTaGCtGAcCGtTTC aAGGCtGAAAAGGTACACTTTGTTTATATTCT GATCGCCAAA
lmn-1(tgx526[E175K]) I	N2	GGCACGCAA CGATAAATT GG AGCCGCCAA CAATAAAAT CA	AAAACAGAAGACGTTGCAGGCACGCAACGATA AATTaGTtGTtaAGAAcGAcGAcCTtAAgAAG CAaAACATtACcCTTCGcGAtACCGTcGAgGG ACTtAAGAAgGCtGTcGAgGATGAgACcCTTC TtCGcACcGCtGCtAACAAcAAgATCAAGGCT CTGGAAGAAGATCTCGCTTTTGCTCTT
lmn-1(tgx535[R204W]) I	N2	ACTCTTCGT GACACCGTA GA TTTGCTCTT CAACAGCAC AA	CTCAAAAAGCAGAACATCACTCTTCGTGACAC CGTtGAgGGACTtAAaAAgGCtGTTGAgGAcG AgACTCTcCTCtGgACAGCtGCCAAtAAcAAg ATtAAGGCcCTtGAgGAgGAcCTtGCcTTTGC cCTcCAgCAaCACAAGGGAGAACTTGAAGAAG TTCGTCACAAGAGAC
lmn-1(tgx539[K284Q]) I	N2	AGCATTGAG CTTGTTTTT GT GACTTGGAG ACATCAAGC AG	GCATCAAAACAAAACAGCTTTCGAAGATGCCT ACAAgAACcAGCTtAAcGCcGCcCGTGAgCGt CAgGAaGAaGCcGTcTCtGAgGCcATtCAcCT caGaGCCaGaGTcaGaGACcTcGAaACcTCcA GCAGTGGAAATGCTTCGCTCATCGAACGTCTT CGTT
lmn-1(tgx561[K331Q] I	N2	GACTTGGAG ACATCAAGC AG CCAAGAGAA GCTCGACGA CA	CTTCGTGCCCGTGTTCGTGACTTGGAGACATC AAGtAGcGGAAAcGCcTCtCTtATtGAgaGaC TTaGaTCtGAaCTtGAtACcCTccAacGtTCt TTCCAgGAaAAGCTtGAtGACAAGGATGCTCG AATTGCTGAACTTAATCAAGAG

lmn-1(tgx397[E358K]) I	N2	CCAAGAGAA GCTCGACGA CA TCTTGAGTT CGGCGTCCA AT	CACTCTGAAGAGATCGTTCCAAGAGAAGCTCG ACGAtAAaGAcGCcCGcATcGCcGAgtTgAAc CAgGAaATtGAaCGaATGATGtcCaAGTTtCA tGActTgtTgGAcGTcAAgATtCAgTTGGACG CCGAACTCAAGACCTACCAAGCTCTCCTTG
lmn-1(tgx390[G407D]) I	N2	GCGTCTCAA TCTTACTCA GG GGAGGAGCA AGCGCTCAG CG	CCTTGAGGGTGAGGAGGAGCGTCTCAATCTTA CTCAaGAGGCaCCgCAgAAtACcTCgGTcCAc CAtGTtTCcTTcTCgTCCGatGGcGCctcCGC cCAGCGCGGAGTGAAGCGTCGTCGCGTTGTCG ATGTAA
lmn-1(tgx529[G528R]) I	N2	AGCATCCGC AGACCAAAC GG GCTCGTCTT GAGGATAGT GA	TCGTATGAAGCTCGCTCCACATGCTAGCGCCA CCGTcTGGTCcGCtGAcGCcGGaGCtGTcCAC CAtCCACCtGAgGTtTACGTcATGAAaAAGCA gCAaTGGCCtATccGtGAcAAtCCATCtGCcC GcCTcGAGGAcAGTGAAGGAGACACTGTTTCT TCTATCACCGTTGAAT
lmn-1(tgx550 [L535P]) I/hT2 (I;III)	N2	CTATCCTCA AGACGAGCT GA GCTCGTCTT GAGGATAGT GA	ACAATTTTCAGTGGCCAATTGGAGATAACCCA TCAGCcCGcCcaGAGGActcTGAAGGAGACAC TGTTTCTTCTATCACCGTTGAAT

[*]All nucleotide sequences are displayed in 5' to 3' orientation.

[†]Lowercase nucleotides differ from the genomic sequence and include the missense, PAM site, and synonymous screening mutations.

[§]Underlined sequences indicate the missense mutation.

Acknowledgements

We thank members of the Starr/Luxton lab for helpful discussions, editing of the paper, and technical help, especially Jamie Ho and Daniel Elnatan for help with imaging. We thank Thomas Wilkop at the MCB Light Microscopy Imaging Facility, which is a UC Davis Campus Core Research Facility, for microscopy assistance.

References

1. Turgay Y, Eibauer M, Goldman AE, Shimi T, Khayat M, Ben-Harush K, et al. The molecular architecture of lamins in somatic cells. Nature. 2017 Mar 1;543(7644):261–4.

2. Shimi T, Kittisopikul M, Tran J, Goldman AE, Adam SA, Zheng Y, et al. Structural organization of nuclear lamins A, C, B1, and B2 revealed by superresolution microscopy. Mol Biol Cell. 2015 Nov 5;26(22):4075–86.

3. Worman HJ. Nuclear lamins and laminopathies. J Pathol. 2012 Jan;226(2):316–25.

4. Worman HJ, Bonne G. "Laminopathies": A wide spectrum of human diseases. Spec Issue - Intermed Filam. 2007 Jun 10;313(10):2121–33.

5. Bertrand AT, Chikhaoui K, Yaou RB, Bonne G. Clinical and genetic heterogeneity in laminopathies. Biochem Soc Trans. 2011 Nov 21;39(6):1687–92.

6. Bonne G, Mercuri E, Muchir A, Urtizberea A, Bécane HM, Recan D, et al. Clinical and molecular genetic spectrum of autosomal dominant Emery-Dreifuss muscular dystrophy due to mutations of the lamin A/C gene. Ann Neurol. 2000 Aug 1;48(2):170–80.

7. Bonne G, Quijano-Roy S. Chapter 142 - Emery–Dreifuss muscular dystrophy, laminopathies, and other nuclear envelopathies. In: Dulac O, Lassonde M, Sarnat HB, editors. Handbook of Clinical Neurology [Internet]. Elsevier; 2013. p. 1367–76. Available from: https://www.sciencedirect.com/science/article/pii/B9780444595652000071

8. Fatkin D, MacRae C, Sasaki T, Wolff MR, Porcu M, Frenneaux M, et al. Missense Mutations in the Rod Domain of the Lamin A/C Gene as Causes of Dilated Cardiomyopathy and Conduction-System Disease. N Engl J Med. 1999 Dec 2;341(23):1715–24.

9. Quijano-Roy S, Mbieleu B, Bönnemann CG, Jeannet PY, Colomer J, Clarke NF, et al. De novo LMNA mutations cause a new form of congenital muscular dystrophy. Ann Neurol. 2008 Aug 1;64(2):177–86.

10. Bonne G, Barletta MRD, Varnous S, Bécane HM, Hammouda EH, Merlini L, et al. Mutations in the gene encoding lamin A/C cause autosomal dominant Emery-Dreifuss muscular dystrophy. Nat Genet. 1999 Mar 1;21(3):285–8.

11. Ben Yaou R, Yun P, Dabaj I, Norato G, Donkervoort S, Xiong H, et al. International retrospective natural history study of LMNA-related congenital muscular dystrophy. Brain Commun. 2021 Jul 1;3(3):fcab075.

12. Scharner J, Brown CA, Bower M, Iannaccone ST, Khatri IA, Escolar D, et al. Novel LMNA mutations in patients with Emery-Dreifuss muscular dystrophy and functional characterization of four LMNA mutations. Hum Mutat. 2011 Feb 1;32(2):152–67.

13. Muchir A, Bonne G, van der Kooi AJ, van Meegen M, Baas F, Bolhuis PA, et al. Identification of mutations in the gene encoding lamins A/C in autosomal dominant limb girdle muscular dystrophy with atrioventricular conduction disturbances (LGMD1B). Hum Mol Genet. 2000 May 22;9(9):1453–9.

14. Benedetti S, Menditto I, Degano M, Rodolico C, Merlini L, D'Amico A, et al. Phenotypic clustering of lamin A/C mutations in neuromuscular patients. Neurology. 2007 Sep 18;69(12):1285.

15. Storey EC, Fuller HR. Genotype-Phenotype Correlations in Human Diseases Caused by Mutations of LINC Complex-Associated Genes: A Systematic Review and Meta-Summary. Cells. 2022;11(24).

16. Anderson CL, Langer ER, Routes TC, McWilliams SF, Bereslavskyy I, Kamp TJ, et al. Most myopathic lamin variants aggregate: a functional genomics approach for assessing variants of uncertain significance. Npj Genomic Med. 2021 Dec 3;6(1):103.

17. Nicolas HA, Hua K, Quigley H, Ivare J, Tesson F, Akimenko MA. A CRISPR/Cas9 zebrafish lamin A/C mutant model of muscular laminopathy. Dev Dyn [Internet]. 2021 Oct 2 [cited 2021 Oct 29];n/a(n/a). Available from: https://doi.org/10.1002/dvdy.427

18. Chandar S, Yeo LS, Leimena C, Tan JC, Xiao XH, Nikolova-Krstevski V, et al. Effects of Mechanical Stress and Carvedilol in Lamin A/C–Deficient Dilated Cardiomyopathy. Circ Res. 2010 Feb 19;106(3):573–82.

19. Mounkes LC, Kozlov S, Hernandez L, Sullivan T, Stewart CL. A progeroid syndrome in mice is caused by defects in A-type lamins. Nature. 2003 May 1;423(6937):298–301.

20. Thomasson R, Vignier N, Peccate C, Mougenot N, Noirez P, Muchir A. Alteration of performance in a mouse model of Emery–Dreifuss muscular dystrophy caused by A-type lamins gene mutation. Hum Mol Genet. 2019 Jul 1;28(13):2237–44.

21. Vignier N, Mougenot N, Bonne G, Muchir A. Effect of genetic background on the cardiac phenotype in a mouse model of Emery-Dreifuss muscular dystrophy. Biochem Biophys Rep. 2019 Sep 1;19:100664.

22. Lyakhovetsky R, Gruenbaum Y. Studying Lamins in Invertebrate Models. In: Schirmer EC, de las Heras JI, editors. Cancer Biology and the Nuclear Envelope: Recent Advances May Elucidate Past Paradoxes [Internet]. New York, NY: Springer New York; 2014. p. 245–62. Available from: https://doi.org/10.1007/978-1-4899-8032-8_11

530 23. Cohen-Fix O, Askjaer P. Cell Biology of the Caenorhabditis elegans Nucleus. Genetics.
531 2017 Jan 1;205(1):25.

532 24. Liu J, Rolef Ben-Shahar T, Riemer D, Treinin M, Spann P, Weber K, et al. Essential roles for
533 Caenorhabditis elegans lamin gene in nuclear organization, cell cycle progression, and spatial
534 organization of nuclear pore complexes. Mol Biol Cell. 2000 Nov;11(11):3937–47.

535 25. Cohen M, Tzur YB, Neufeld E, Feinstein N, Delannoy MR, Wilson KL, et al. Transmission electron
536 microscope studies of the nuclear envelope in Caenorhabditis elegans embryos. J Struct Biol. 2002
537 Oct 1;140(1):232–40.

538 26. Gruenbaum Y, Lee KK, Liu J, Cohen M, Wilson KL. The expression, lamin-dependent localization
539 and RNAi depletion phenotype for emerin in C. elegans. J Cell Sci. 2002 Mar 1;115(5):923–9.

540 27. Liu J, Lee KK, Segura-Totten M, Neufeld E, Wilson KL, Gruenbaum Y. MAN1 and emerin have
541 overlapping function(s) essential for chromosome segregation and cell division in Caenorhabditis
542 elegans. Proc Natl Acad Sci. 2003 Apr 15;100(8):4598–603.

543 28. Margalit A, Neufeld E, Feinstein N, Wilson KL, Podbilewicz B, Gruenbaum Y. Barrier to
544 autointegration factor blocks premature cell fusion and maintains adult muscle integrity in C.
545 elegans. J Cell Biol. 2007 Aug 13;178(4):661–73.

546 29. Lee KK, Starr D, Cohen M, Liu J, Han M, Wilson KL, et al. Lamin-dependent Localization of
547 UNC-84, A Protein Required for Nuclear Migration in Caenorhabditis elegans. Mol Biol Cell. 2002
548 Mar 1;13(3):892–901.

549 30. Zuela N, Zwerger M, Levin T, Medalia O, Gruenbaum Y. Impaired mechanical response of an
550 EDMD mutation leads to motility phenotypes that are repaired by loss of prenylation. J Cell Sci.
551 2016 Jan 1;jcs.184309.

552 31. Mattout A, Pike BL, Towbin BD, Bank EM, Gonzalez-Sandoval A, Stadler MB, et al. An EDMD
553 Mutation in C. elegans Lamin Blocks Muscle-Specific Gene Relocation and Compromises Muscle
554 Integrity. Curr Biol. 2011 Oct 11;21(19):1603–14.

555 32. Bank EM, Ben-Harush K, Wiesel-Motiuk N, Barkan R, Feinstein N, Lotan O, et al. A laminopathic
556 mutation disrupting lamin filament assembly causes disease-like phenotypes in Caenorhabditis
557 elegans. Mol Biol Cell. 2011 Aug 1;22(15):2716–28.

558 33. Wiesel N, Mattout A, Melcer S, Melamed-Book N, Herrmann H, Medalia O, et al. Laminopathic
559 mutations interfere with the assembly, localization, and dynamics of nuclear lamins. Proc Natl Acad
560 Sci U S A. 2007/12/27 ed. 2008 Jan 8;105(1):180–5.

561 34. Bank EM, Gruenbaum Y. Caenorhabditis elegans as a model system for studying the nuclear lamina
562 and laminopathic diseases. Nucleus. 2011 Sep 1;2(5):350–7.

563 35. Bone CR, Chang YT, Cain NE, Murphy SP, Starr DA. Nuclei migrate through constricted spaces
564 using microtubule motors and actin networks in C. elegans hypodermal cells. Development. 2016
565 Nov 15;143(22):4193–202.

566 36. Wu X, Wang QK, Gui L, Liu M, Zhang X, Jin R, et al. Identification of a new lamin A/C mutation
567 in a chinese family affected with atrioventricular block as the prominent phenotype. J Huazhong
568 Univ Sci Technolog Med Sci. 2010 Feb 1;30(1):103–7.

569 37. Wang H, Wang J, Zheng W, Wang X, Wang S, Song L, et al. Mutation Glu82Lys in lamin A/C
570 gene is associated with cardiomyopathy and conduction defect. Biochem Biophys Res Commun.
571 2006 May 26;344(1):17–24.

572 38. Lin XF, Luo JW, Liu G, Zhu YB, Jin Z, Lin X. Genetic mutation of familial dilated cardiomyopathy
573 based on next-generation semiconductor sequencing. Mol Med Rep. 2018/09/05 ed. 2018
574 Nov;18(5):4271–80.

575 39. Sébillon P, Bouchier C, Bidot LD, Bonne G, Ahamed K, Charron P, et al. Expanding the phenotype
576 of LMNA mutations in dilated cardiomyopathy and functional consequences of these mutations. J
577 Med Genet. 2003 Aug;40(8):560–7.

578 40. Song K, Dube MP, Lim J, Hwang I, Lee I, Kim JJ. Lamin A/C mutations associated with familial
579 and sporadic cases of dilated cardiomyopathy in Koreans. Exp Mol Med. 2007 Feb 1;39(1):114–20.

580 41. Pasotti M, Klersy C, Pilotto A, Marziliano N, Rapezzi C, Serio A, et al. Long-Term Outcome and
581 Risk Stratification in Dilated Cardiolaminopathies. J Am Coll Cardiol. 2008 Oct 7;52(15):1250–60.

582 42. Perrot A, Hussein S, Ruppert V, Schmidt HHJ, Wehnert MS, Duong NT, et al. Identification of
583 mutational hot spots in LMNA encoding lamin A/C in patients with familial dilated
584 cardiomyopathy. Basic Res Cardiol. 2009 Jan 1;104(1):90–9.

585 43. Arbustini E, Pilotto A, Repetto A, Grasso M, Negri A, Diegoli M, et al. Autosomal dominant dilated
586 cardiomyopathy with atrioventricular block: a lamin A/C defect-related disease. J Am Coll Cardiol.
587 2002 Mar 20;39(6):981–90.

588 44. Hermida-Prieto M, Monserrat L, Castro-Beiras A, Laredo R, Soler R, Peteiro J, et al. Familial
589 dilated cardiomyopathy and isolated left ventricular noncompaction associated with lamin A/C gene
590 mutations. Am J Cardiol. 2004 Jul 1;94(1):50–4.

591 45. Pethig K, Genschel J, Peters T, Wilhelmi M, Flemming P, Lochs H, et al. LMNA Mutations in
592 Cardiac Transplant Recipients. Cardiology. 2005;103(2):57–62.

593 46. Sylvius N, Bilinska ZT, Veinot JP, Fidzianska A, Bolongo PM, Poon S, et al. In vivo and in vitro
594 examination of the functional significances of novel lamin gene mutations in heart failure patients. J
595 Med Genet. 2005 Aug;42(8):639–47.

596 47. Kärkkäinen S, Reissell E, Heliö T, Kaartinen M, Tuomainen P, Toivonen L, et al. Novel mutations
597 in the lamin A/C gene in heart transplant recipients with end stage dilated cardiomyopathy. Heart.
598 2006 Apr 1;92(4):524.

599 48. Quarta G, Syrris P, Ashworth M, Jenkins S, Zuborne Alapi K, Morgan J, et al. Mutations in the
600 Lamin A/C gene mimic arrhythmogenic right ventricular cardiomyopathy. Eur Heart J. 2012 May
601 1;33(9):1128–36.

602 49. Millat G, Bouvagnet P, Chevalier P, Sebbag L, Dulac A, Dauphin C, et al. Clinical and mutational
603 spectrum in a cohort of 105 unrelated patients with dilated cardiomyopathy. Eur J Med Genet. 2011
604 Nov 1;54(6):e570–5.

605 50. Dal Ferro M, Stolfo D, Altinier A, Gigli M, Perrieri M, Ramani F, et al. Association between
606 mutation status and left ventricular reverse remodelling in dilated cardiomyopathy. Heart. 2017 Nov
607 1;103(21):1704.

608 51. Kuruc JC, Durant-Archibold AA, Motta J, Rao KS, Trachtenberg B, Ramos C, et al. Development
609 of anthracycline-induced dilated cardiomyopathy due to mutation on LMNA gene in a breast cancer
610 patient: a case report. BMC Cardiovasc Disord. 2019 Jul 16;19(1):169–169.

611 52. Pasqualin LMA, Reed UC, Costa TVMM, Quedas E, Albuquerque MAV, Resende MBD, et al.
612 Congenital Muscular Dystrophy With Dropped Head Linked to the LMNA Gene in a Brazilian
613 Cohort. Pediatr Neurol. 2014 Apr 1;50(4):400–6.

614 53. Tan D, Yang H, Yuan Y, Bonnemann C, Chang X, Wang S, et al. Phenotype–Genotype Analysis of
615 Chinese Patients with Early-Onset LMNA-Related Muscular Dystrophy. PLOS ONE. 2015 Jun
616 22;10(6):e0129699.

617 54. Brown CA, Lanning RW, McKinney KQ, Salvino AR, Cherniske E, Crowe CA, et al. Novel and
618 recurrent mutations in lamin A/C in patients with Emery-Dreifuss muscular dystrophy. Am J Med
619 Genet. 2001 Sep 1;102(4):359–67.

620 55. Mercuri E, Poppe M, Quinlivan R, Messina S, Kinali M, Demay L, et al. Extreme Variability of
621 Phenotype in Patients With an Identical Missense Mutation in the Lamin A/C Gene: From
622 Congenital Onset With Severe Phenotype to Milder Classic Emery-Dreifuss Variant. Arch Neurol.
623 2004 May 1;61(5):690–4.

624 56. Sewry CA, Brown SC, Mercuri E, Bonne G, Feng L, Camici G, et al. Skeletal muscle pathology in
625 autosomal dominant Emery-Dreifuss muscular dystrophy with lamin A/C mutations. Neuropathol
626 Appl Neurobiol. 2001 Aug 1;27(4):281–90.

627 57. Liang WC, Tian X, Yuo CY, Chen WZ, Kan TM, Su YN, et al. Comprehensive target capture/next-
628 generation sequencing as a second-tier diagnostic approach for congenital muscular dystrophy in
629 Taiwan. PLOS ONE. 2017 Feb 9;12(2):e0170517.

630 58. Le Thanh P, Meinke P, Korfali N, Srsen V, Robson MI, Wehnert M, et al. Immunohistochemistry
631 on a panel of Emery–Dreifuss muscular dystrophy samples reveals nuclear envelope proteins as
632 inconsistent markers for pathology. Neuromuscul Disord. 2017 Apr 1;27(4):338–51.

633 59. Karczewski KJ, Francioli LC, Tiao G, Cummings BB, Alföldi J, Wang Q, et al. The mutational
634 constraint spectrum quantified from variation in 141,456 humans. Nature. 2020 May
635 1;581(7809):434–43.

636 60. Landrum MJ, Lee JM, Benson M, Brown GR, Chao C, Chitipiralla S, et al. ClinVar: improving
637 access to variant interpretations and supporting evidence. Nucleic Acids Res. 2018 Jan
638 4;46(D1):D1062–7.

639 61. Pugh TJ, Kelly MA, Gowrisankar S, Hynes E, Seidman MA, Baxter SM, et al. The landscape of
640 genetic variation in dilated cardiomyopathy as surveyed by clinical DNA sequencing. Genet Med.
641 2014 Aug 1;16(8):601–8.

642 62. Fichna JP, Macias A, Piechota M, Korostyński M, Potulska-Chromik A, Redowicz MJ, et al.
643 Whole-exome sequencing identifies novel pathogenic mutations and putative phenotype-influencing
644 variants in Polish limb-girdle muscular dystrophy patients. Hum Genomics. 2018 Jul 3;12(1):34–34.

645 63. Møller DV, Pham TT, Gustafsson F, Hedley P, Ersbøll MK, Bundgaard H, et al. The role of Lamin
646 A/C mutations in Danish patients with idiopathic dilated cardiomyopathy. Eur J Heart Fail. 2009
647 Nov 1;11(11):1031–5.

648 64. van Spaendonck-Zwarts KY, van Rijsingen IAW, van den Berg MP, Lekanne Deprez RH, Post JG,
649 van Mil AM, et al. Genetic analysis in 418 index patients with idiopathic dilated cardiomyopathy:
650 overview of 10 years' experience. Eur J Heart Fail. 2013 Jun 1;15(6):628–36.

651 65. Dalin MG, Engström PG, Ivarsson EG, Unneberg P, Light S, Schaufelberger M, et al. Massive
652 parallel sequencing questions the pathogenic role of missense variants in dilated cardiomyopathy.
653 Int J Cardiol. 2017 Feb 1;228:742–8.

654 66. Hoorntje ET, Bollen IA, Barge-Schaapveld DQ, van Tienen FH, te Meerman GJ, Jansweijer JA, et
655 al. Lamin A/C-Related Cardiac Disease. Circ Cardiovasc Genet. 2017 Aug 1;10(4):e001631.

67. Hasselberg NE, Haland TF, Saberniak J, Brekke PH, Berge KE, Leren TP, et al. Lamin A/C cardiomyopathy: young onset, high penetrance, and frequent need for heart transplantation. Eur Heart J. 2018 Mar 7;39(10):853–60.

68. Torvaldson E, Kochin V, Eriksson JE. Phosphorylation of lamins determine their structural properties and signaling functions. Nucleus. 2015 May 4;6(3):166–71.

69. Haithcock E, Dayani Y, Neufeld E, Zahand AJ, Feinstein N, Mattout A, et al. Age-related changes of nuclear architecture in Caenorhabditis elegans. Proc Natl Acad Sci U S A. 2005/11/03 ed. 2005 Nov 15;102(46):16690–5.

70. Harr JC, Schmid CD, Muñoz-Jiménez C, Romero-Bueno R, Kalck V, Gonzalez-Sandoval A, et al. Loss of an H3K9me anchor rescues laminopathy-linked changes in nuclear organization and muscle function in an Emery-Dreifuss muscular dystrophy model. Genes Dev. 2020/03/05 ed. 2020 Apr 1;34(7–8):560–79.

71. Bone CR, Tapley EC, Gorjánácz M, Starr DA. The Caenorhabditis elegans SUN protein UNC-84 interacts with lamin to transfer forces from the cytoplasm to the nucleoskeleton during nuclear migration. Mol Biol Cell. 2014 Sep 15;25(18):2853–65.

72. Fridolfsson HN, Herrera LA, Brandt JN, Cain NE, Hermann GJ, Starr DA. Genetic Analysis of Nuclear Migration and Anchorage to Study LINC Complexes During Development of Caenorhabditis elegans. In: Gundersen GG, Worman HJ, editors. The LINC Complex: Methods and Protocols [Internet]. New York, NY: Springer New York; 2018. p. 163–80. Available from: https://doi.org/10.1007/978-1-4939-8691-0_13

73. Starr DA, Hermann GJ, Malone CJ, Fixsen W, Priess JR, Horvitz HR, et al. unc-83 encodes a novel component of the nuclear envelope and is essential for proper nuclear migration. Development. 2001 Dec 15;128(24):5039–50.

679 74. Cao K, Capell BC, Erdos MR, Djabali K, Collins FS. A lamin A protein isoform overexpressed in
680 Hutchinson-Gilford progeria syndrome interferes with mitosis in progeria and normal cells. Proc
681 Natl Acad Sci U S A. 2007/03/14 ed. 2007 Mar 20;104(12):4949–54.

682 75. Goldman RD, Shumaker DK, Erdos MR, Eriksson M, Goldman AE, Gordon LB, et al.
683 Accumulation of mutant lamin A causes progressive changes in nuclear architecture in Hutchinson–
684 Gilford progeria syndrome. Proc Natl Acad Sci. 2004 Jun 15;101(24):8963.

685 76. Chen CY, Chi YH, Mutalif RA, Starost MF, Myers TG, Anderson SA, et al. Accumulation of the
686 Inner Nuclear Envelope Protein Sun1 Is Pathogenic in Progeric and Dystrophic Laminopathies.
687 Cell. 2012 Apr 27;149(3):565–77.

688 77. Uchino R, Nonaka Y ki, Horigome T, Sugiyama S, Furukawa K. Loss of Drosophila A-type lamin
689 C initially causes tendon abnormality including disintegration of cytoskeleton and nuclear lamina in
690 muscular defects. Dev Biol. 2013 Jan 1;373(1):216–27.

691 78. Bank EM, Ben-Harush K, Feinstein N, Medalia O, Gruenbaum Y. Structural and physiological
692 phenotypes of disease-linked lamin mutations in C. elegans. Ueli Aebi Festschr. 2012 Jan
693 1;177(1):106–12.

694 79. Östlund C, Bonne G, Schwartz K, Worman HJ. Properties of lamin A mutants found in Emery-
695 Dreifuss muscular dystrophy, cardiomyopathy and Dunnigan-type partial lipodystrophy. J Cell Sci.
696 2001 Dec 15;114(24):4435–45.

697 80. Davidson PM, Lammerding J. Broken nuclei – lamins, nuclear mechanics, and disease. Trends Cell
698 Biol. 2014 Apr 1;24(4):247–56.

699 81. Sullivan T, Escalante-Alcalde D, Bhatt H, Anver M, Bhat N, Nagashima K, et al. Loss of A-type
700 lamin expression compromises nuclear envelope integrity leading to muscular dystrophy. J Cell
701 Biol. 1999 Nov 29;147(5):913–20.

702 82. Muchir A, Medioni J, Laluc M, Massart C, Arimura T, Kooi AJVD, et al. Nuclear envelope
703 alterations in fibroblasts from patients with muscular dystrophy, cardiomyopathy, and partial
704 lipodystrophy carrying lamin A/C gene mutations. Muscle Nerve. 2004 Oct 1;30(4):444–50.

705 83. Fidziańska A, Hausmanowa-Petrusewicz I. Architectural abnormalities in muscle nuclei.
706 Ultrastructural differences between X-linked and autosomal dominant forms of EDMD. J Neurol
707 Sci. 2003 Jun 15;210(1):47–51.

708 84. Zwerger M, Jaalouk DE, Lombardi ML, Isermann P, Mauermann M, Dialynas G, et al. Myopathic
709 lamin mutations impair nuclear stability in cells and tissue and disrupt nucleo-cytoskeletal coupling.
710 Hum Mol Genet. 2013/02/19 ed. 2013 Jun 15;22(12):2335–49.

711 85. Shaw NM, Rios-Monterrosa JL, Fedorchak GR, Ketterer MR, Coombs GS, Lammerding J, et al.
712 Effects of mutant lamins on nucleo-cytoskeletal coupling in Drosophila models of LMNA muscular
713 dystrophy. Front Cell Dev Biol [Internet]. 2022;10. Available from:
714 https://www.frontiersin.org/articles/10.3389/fcell.2022.934586

715 86. Zhou C, Li C, Zhou B, Sun H, Koullourou V, Holt I, et al. Novel nesprin-1 mutations associated
716 with dilated cardiomyopathy cause nuclear envelope disruption and defects in myogenesis. Hum
717 Mol Genet. 2017 Jun 15;26(12):2258–76.

718 87. Brenner S. THE GENETICS OF CAENORHABDITIS ELEGANS. Genetics. 1974 May
719 1;77(1):71–94.

720 88. Arribere JA, Bell RT, Fu BXH, Artiles KL, Hartman PS, Fire AZ. Efficient Marker-Free Recovery
721 of Custom Genetic Modifications with CRISPR/Cas9 in Caenorhabditis elegans. Genetics. 2014
722 Nov 1;198(3):837–46.

723 89. Paix A, Folkmann A, Rasoloson D, Seydoux G. High Efficiency, Homology-Directed Genome
724 Editing in Caenorhabditis elegans Using CRISPR-Cas9 Ribonucleoprotein Complexes. Genetics.
725 2015 Sep 1;201(1):47–54.

726 90. Paix A, Folkmann A, Seydoux G. Precision genome editing using CRISPR-Cas9 and linear repair
727 templates in C. elegans. CRISPR-Cas Syst Genome Eng Investig. 2017 May 15;121–122:86–93.

728 91. Farboud B, Meyer BJ. Dramatic Enhancement of Genome Editing by CRISPR/Cas9 Through
729 Improved Guide RNA Design. Genetics. 2015 Apr 1;199(4):959–71.

730 92. Hao H, Kalra S, Jameson LE, Guerrero LA, Cain NE, Bolivar J, et al. The Nesprin-1/-2 ortholog
731 ANC-1 regulates organelle positioning in C. elegans independently from its KASH or actin-binding
732 domains. Parsons M, Sengupta P, Jantsch V, editors. eLife. 2021 Apr 16;10:e61069.

733 93. Schindelin J, Arganda-Carreras I, Frise E, Kaynig V, Longair M, Pietzsch T, et al. Fiji: an open-
734 source platform for biological-image analysis. Nat Methods. 2012 Jul 1;9(7):676–82.

735 94. AU - Nussbaum-Krammer CI, AU - Neto MF, AU - Brielmann RM, AU - Pedersen JS, AU -
736 Morimoto RI. Investigating the Spreading and Toxicity of Prion-like Proteins Using the Metazoan
737 Model Organism C. elegans. J Vis Exp. 2015 Jan 8;(95):e52321.

738 95. McGee MD, Stagljar I, Starr DA. KDP-1 is a nuclear envelope KASH protein required for cell-
739 cycle progression. J Cell Sci. 2009 Aug 15;122(16):2895–905.

96. Morales-Martínez A, Dobrzynska A, Askjaer P. Inner nuclear membrane protein LEM-2 is required for correct nuclear separation and morphology in C. elegans. J Cell Sci. 2015 Mar 15;128(6):1090–6.

97. Lawrence KS, Tapley EC, Cruz VE, Li Q, Aung K, Hart KC, et al. LINC complexes promote homologous recombination in part through inhibition of nonhomologous end joining. J Cell Biol. 2016 Dec 12;215(6):801–21.

Supporting information

S1 File. Wild-type Animals Exhibit Robust Swimming Behavior. An example video of L4 stage *C. elegans* swimming in buffer for 30 seconds. The number of body bends is shown in gray text next to each animal and was generated by the Fiji wrMTrck plugin.

S2 File. Homozygous *lmn-1(Y59C)* Animals have Impaired Motility. A representative video of homozygous *lmn-1(Y59C)* L4 stage animals thrashing in buffer for 30 seconds. The number of body bends is shown in gray text next to each animal and was generated by the Fiji wrMTrck plugin.

S3 File. Homozygous *lmn-1(R64P)* Animals Demonstrate Swimming Behavior Ranging from Normal to No Motility. An example video of homozygous *lmn-1(R64P)* L4 stage animals swimming in buffer for 30 seconds. The number of body bends is shown in gray text next to each animal and was generated by the Fiji wrMTrck plugin.

S4 File. A VUS, *lmn-1(K331Q)*, Significantly Reduces Swimming Motility in *C. elegans*. A representative video of *lmn-1(K331Q)* L4 animals thrashing in buffer for 30 seconds. The number of body bends is shown in gray text next to each animal and was generated by the Fiji wrMTrck plugin.

760 **S5 File. Homozygous *lmn-1(L535P)* animals have the most severe swimming defect.** An example

761 video of homozygous *lmn-1(L535P)* animals swimming in buffer for 30 seconds. The number of body

762 bends is shown in gray text next to each animal and was generated by the Fiji wrMTrck plugin.

763